

Large Scale Synthesis of Tellurium Nanoribbons in Tetraethylene Pentamine Aqueous Solution and the Stability of Tellurium Nanoribbons in Ethanol and Water

Zhubing He and Shu-Hong Yu*

Division of Nanomaterials & Chemistry, Hefei National Laboratory for Physical Sciences at Microscale, Structural Research Laboratory of CAS, School of Chemistry & Materials, University of Science and Technology of China, Hefei 230026, P. R. China

Received: August 9, 2005; In Final Form: September 30, 2005

Superlong single crystal tellurium nanoribbons with a width of 200–300 nm and length up to several hundred micrometers have been synthesized in tetraethylene pentamine aqueous solution at 80 °C. The stability of as prepared tellurium nanoribbons in solvents such as pure ethanol and deionized water has been studied. The poor crystallinity of the initial single crystalline Te nanoribbons with prolonged storing time demonstrated that the initial single crystalline nanobelts tend to be destroyed and to dissolve in the solvent. In meantime, the supersaturation of the solvable Te species in such solvents will result in the formation of amorphous Te, and the formation of amorphous TeO₂ due to partial oxidation of the Te nanostructures and the newly formed amorphous Te. The detailed corrosion process, crystallinity, and shape evolution process have been carefully examined by the XRD, TEM, HRTEM, and XPS techniques. This erosion phenomenon attacked by solvents has been not identified previously, suggesting that tellurium nanoribbons synthesized by other chemical methods could be also not stable in solution system and their storage after laboratory synthesis requires special attention.

Introduction

One-dimensional nanostructures of functional materials have attracted more and more attention from scientists and engineers, as they can be used in the fabrication of nanodevices. As a narrow band gap semiconductor, tellurium exhibits many potential properties, such as photoconductivity, nonlinear optical response, thermoelectric reactivity, and an effect of superfast electronic excitation on the A₁ phonon frequency, resulting in their applications in electronic and optical electronic devices.¹ Many methodologies have been developed for the syntheses of elemental tellurium nanostructures, for example, electrochemical and electrophoretic deposition² and physical evaporation.³ A self-seeding growth regime was utilized to illustrate the synthesis of tellurium nanorods, nanowires, and nanotubes.⁴ Helical nanobelts and nanotubes based on belt–roll–growth mechanisms were made.⁵ Under high alkaline and acidic conditions, nanowires and nanotubes were also fabricated by solvothermal method,⁶ in which surfactants played an important role in morphology shaping. Under high alkaline solution, rigid tellurium nanotubes were synthesized in hydrazine by a solvothermal method.⁷ Gautam et al. reported a hydrothermal route to prepare Y-junction nanowires in the presence of a strong reducing reagent NaBH₄.⁸ Surfactant trioctylphosphine oxide (TOPO) was also utilized as a good surfactant to form uniform nanowires in polydecene at 203 °C.⁹ Microwave-assisted synthesis of tellurium reduced the necessary temperature in glycol solvents to 80 °C.¹⁰ Ionic liquid was taken as template for preparing tellurium nanowires and nanorods, in which *N*-butylpyridinium tetrafluoroborate and PVP were applied in the synthesis.¹¹ Chemical decomposition of stabilizer-depleted CdTe nanoparticles in the presence of a strong complexing agent results in the formation of highly crystalline Te nanowires.¹²

Other bioorganic molecules have also been utilized to shape the growth of one-dimensional tellurium nanowires.¹³ Recently, our group has used biomolecules as additives to produce scrolled nanotubes and nanowires with sharp ends.¹⁴

These methods offered flexible routes to prepare one-dimensional structures with different shapes and structural features. Nevertheless, low cost and easy controlling synthetic routes are still needed. Additionally, it is critical to examine whether these tellurium nanostructures in various forms are stable or not in solutions from the viewpoint of applications; however, there has been no investigation performed on this issue.

In this paper, we report a facile route to prepare uniform superlong tellurium nanoribbons at low temperature and the stability of the nanoribbons in solvents. Tetraethylene pentamine aqueous solution can reduce telluride to elemental tellurium under mild conditions. The shape evolution process of single crystalline nanoribbons has been investigated. The stability of as-prepared nanoribbons in different solvents has been studied for the first time.

Experimental Section

Synthesis of Superlong Tellurium Nanoribbons. All chemicals are used as received without further purification. In a typical synthesis procedure, 0.025 mmol of sodium telluride was dissolved into 12.5 mL of distilled water, and then the solution mixed with 12.5 mL of tetraethylene pentamine (AC) was vigorously stirred in a wide mouthed reagent bottle for half an hour. Finally, the bottle was sealed with PARAFILM and placed into a bake oven at 80 °C for different times. After 1.5 h, the solution turned dark blue. Subsequently, an obvious floccule floated throughout the whole solution after 8 h and a cloudy flocculent came into being finally with a transparent yellow solution when left alone. The product was washed with ethanol several times and preserved in sample takers.

* Correspondence should be addressed to S. H. Yu, Fax: + 86 551 3603040, Email: shyu@ustc.edu.cn.

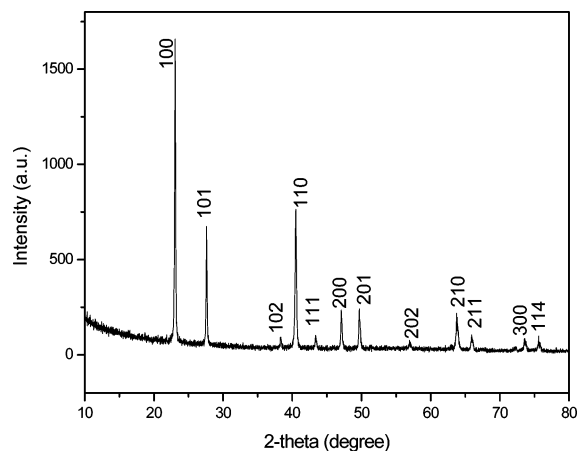


Figure 1. XRD pattern of the product synthesized using 0.02 mmol NaTeO₃ in 25 mL aqueous tetraethylene pentamine solution at 80 °C. The volume ratio of distilled water and tetraethylene pentamine is 1:1.

The Stability and Corrosion of Nanoribbons in Different Solvents. For stability study, a certain amount of fresh prepared tellurium nanoribbons was put into two 50 mL weighing bottles, respectively, one for pure ethanol and the other for deionized water. They are kept for different times and the intermediates after different storing times were sampled for characterization.

Characterization. The structure of these obtained samples were characterized by the X-ray diffraction pattern (XRD), which was recorded on a MAC Science Co. Ltd. MXP 18 AHF X-ray diffractometer with monochromatized Cu K α radiation ($\lambda = 1.54056 \text{ \AA}$). Transmission electron microscopy (TEM) and high-resolution transmission electron microscopy (HRTEM), were performed on a Hitachi (Tokyo, Japan) H-800 transmission electron microscope (TEM) at an accelerating voltage of 200 kV, and a JEOL-2010 high-resolution transmission electron microscope (HRTEM), also at 200 kV, respectively. Scanning electron microscope (SEM) measurements were carried out with a field-emission microscope (JEOL, 7500B) operated at an acceleration voltage of 10 kV. The IR spectra were measured on a Bruker Vector-22 FT-IR spectrometer at room temperature. The ingredients of the sample were detected by X-ray photoelectron spectroscopy (XPS) technique, which was operated on VG ESCALAB MKII with monochromatized Mg K α radiation.

Results and Discussion

Synthesis of Single Crystalline Te Nanoribbons. Hydrazine was used as the reducing agent to reduce positive valence of tellurium under flux⁴ and solvothermal conditions.⁶ Aqueous ammonia was also taken as solvent to synthesize tellurium nanotubes and nanobelts,⁵ where it acts as not only a solvent, but also a reactant, which plays a crucial role in reducing tellurate into elemental tellurium. In the present case, tellurium colloids turned out after only 1.5 h in aqueous tetraethylene pentamine solvent at 80 °C. Obvious floccule can be obtained after reaction for 8 h. It has to be pointed out that not all the amines can reduce tellurate to elemental tellurium, and only amines with multiamino groups are able to yield elemental tellurium. In present work, using either tetraethylene pentamine or diethanol triamine can produce tellurium.

Figure 1 shows that the product is well crystallized elemental tellurium. All the diffraction peaks can be indexed as trigonal tellurium phase (JCPDS 36-1452). The enhanced relative intensities of 100 and 110 diffraction peaks compared with those for the standard indicated the possible preferential orientation. The SEM image in Figure 2a shows that the floccule is

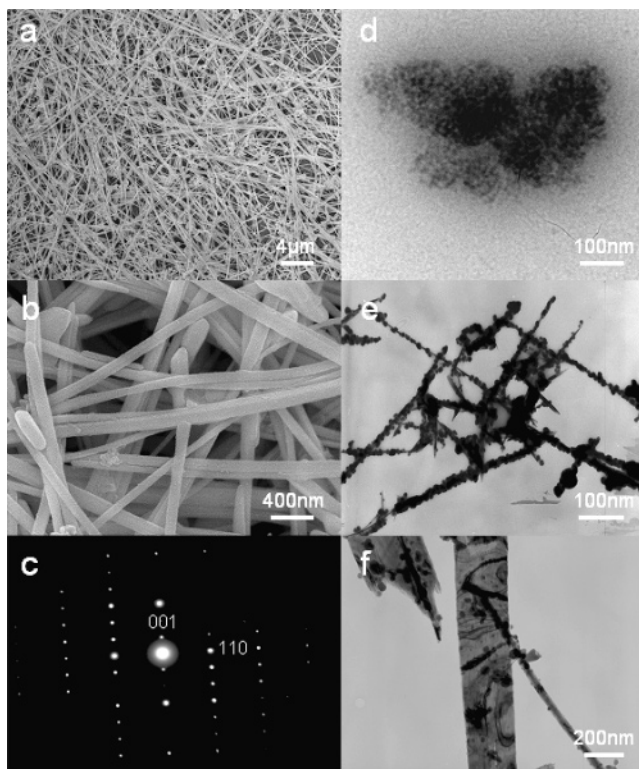


Figure 2. SEM and TEM images of the sample synthesized with 0.02 mmol NaTeO₃ in 25 mL aqueous tetraethylene pentamine (the volume ratio of distilled water and tetraethylene pentamine is 1:1) at 80 °C for different time. (a, b) low and high magnification of FESEM images of the sample for 4 days. (c) electron diffraction pattern taken on a single nanoribbon. (d, e) TEM images of the samples obtained after reaction for 4 h and 24 h, respectively. (f) TEM image of the sample obtained after reaction for 4 days.

composed of ultralong nanoribbons of tellurium with lengths of several micrometers and widths of 200–300 nm as clearly observed in the high magnification SEM image (Figure 2b). The selected area diffraction pattern in Figure 2c was taken on a typical individual nanobelt, showing that the nanobelt is single crystalline with growth direction along [001]. The IR spectrum of the freshly prepared sample does not show the presence of any tetraethylene pentamine.

Time dependent growth process of nanobelts was investigated. Amorphous particles formed after 4 h (Figure 2d). Because of their own high thermodynamic level, these amorphous particles tend to grow into nanowires of trigonal tellurium owing to its 3₁ helical-chain in structure. The formation of amorphous nanoparticles formed rapidly by reducing sodium telluride with tetraethylene pentamine is consistent with that previous report.⁴ With time prolonged, the nanoparticles tend to form wirelike nanostructures on which a lot of nanoparticles adsorbed after reaction for 24 h (Figure 2e). In the end, the beads-stringlike nanostructures ripened into nanobelts at consumption of these adsorbed nanoparticles as shown in Figure 2f.

The concentration of sodium telluride has significant effects on the formation of nanostructures. A low concentration of sodium telluride favors the formation of nanobelts rather than nanowires. The influence of the concentration on the nanostructures was illustrated in Figure 3. When the concentration decreased to 0.05 mmol, nanobelts turned out in the final product (Figure 3c). Moreover, the diameter of nanowires declined with the concentration decreasing as Figure 3b,c shows.

Stability of Te Nanoribbons in Different Solvents. The nanoribbons were not stable when they are stored in solvents

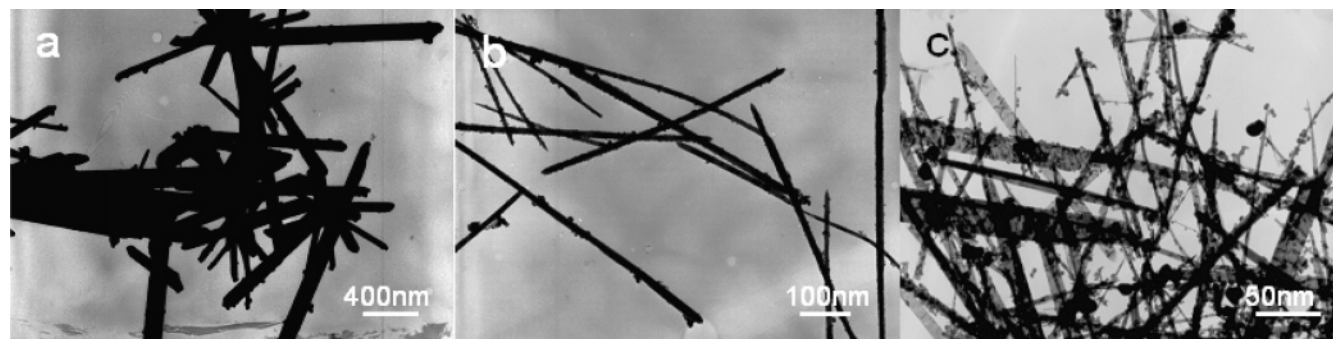


Figure 3. TEM images of the samples obtained at 80 °C using different concentration of sodium telluride. (a–c) The concentration of sodium telluride is 0.5, 0.1, and 0.05 mmol sodium telluride, respectively. The reaction was done in 25 mL aqueous tetraethylene pentamine solution with the volume ratio of 1:1 (distilled water and tetraethylene pentamine).

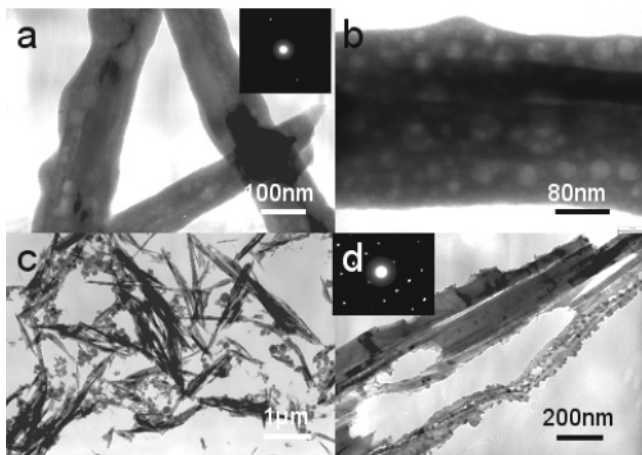


Figure 4. TEM images of rotten tellurium nanoribbons in pure ethanol and deionized water for 35 days, respectively. (a, b) Typical morphology of structures which were penetrated by pure ethanol is shown. The inserted ED taken on the structures, showing that the structures are amorphous. (c, d) Typical TEM images of the gnawed structures by water are shown. The inserted ED pattern shows that the remaining part of the nanoribbons is still single crystalline.

such as pure ethanol or deionized water. This observation is not consistent with a previous report that tellurium nanotubes remained unchanged in water or ethanol for several months.⁴

The morphology of the rotten nanoribbons in ethanol and water after storing in these two solvents for 35 days is shown in Figure 4. Higher magnification TEM images show that the smooth surface of the initial intact nanoribbons becomes rough and there are a lot of holes within the nanoribbon body (Figure 4a,b). The ethanol molecules could invade into the backbone of the nanoribbon (Figure 4b). The selected area diffraction pattern taken on the wires shows an amorphous feature (inset in Figure 5a). In contrast, the sample obtained after eroding in water for the same period shows different features as that above observed in ethanol (Figure 4c,d). The long nanoribbons become shorter and the obvious eroding event happened in a way that is different from in ethanol. In addition, the electron diffraction pattern taken on the backbone of the eroded nanoribbon shows that it is still single crystalline (inset in Figure 4d).

To further understand the initial stages of the eroding process, the samples after eroding for 15 days were obtained for TEM, HRTEM, and XRD analysis. High-resolution TEM images in Figure 5 reveal the detailed structural features during the eroding process, which were taken on the samples after eroding for 15 days in ethanol. Figure 5a shows the initial stage of erosion happened on the nanoribbons. Figure 5b,c,d shows the HRTEM images selected on an eroded nanoribbon (shown in Figure 5a) which were taken on the different positions of the nanoribbon

(in 1, 2, 3 order marked as three white panes). At the tip of the damaged nanoribbon, no crystal lattice fringes can be observed (Figure 5b). However, the lattice fringes with a spacing of 5.90 Å can be observed on the trunk of the ribbon, corresponding to the growth direction along [001] (Figure 5c). The lattice fringes with a spacing of 2.23 Å, which are perpendicular to those of (001) plane, are corresponding to that of (110) plane. However, the lattice fringes with a spacing of 3.24 Å are frequently observed, corresponding to that of (101) plane. Additionally, an amorphous layer of a thickness of about 25 nm coexisted with the destroyed backbone was observed. Furthermore, a lot of jags were observed and they already extended along the whole backbone of the ribbon, which can be confirmed by the contrast difference of the TEM image.

However, this observation is different from what the erosion event took place in water. Although an amorphous layer also yielded around the ribbon, but the eroded notches are observed along the backbone and they turned along it, the key difference between them is that bone structure eroded in water keep intact as a fresh one with conspicuous lattice fringes of spacing 5.90 Å for (001) plane (Figure 6b,c). Also an amorphous layer was observed (Figure 6b). The result suggested that polar water molecules could only attack from surface along the backbone of the nanoribbons gradually rather than that ethanol molecules can penetrate into the backbone.

The erosion process and the crystallinity of the intermediates in the two solvents were respectively examined by time dependent XRD measurement (Figure 7). The intermediate samples after storing for different time were also examined by HRTEM. The XRD pattern for the initial nanoribbons shows that there are three intensive diffraction peaks (100), (101), (110) are observed and the (100) peak is the strongest and (101) plane is weakest (Figure 7a). Compared with the XRD pattern for the initial single crystalline tellurium (Figure 7a), the intensities of the diffraction peaks for the product after storing in ethanol for 15 days become weaker. Two distinguished features are observed based on the XRD patterns. First, the (100), (110) peaks became weaker and (101) and became more intensified. As we discussed above, the nanoribbons were attacked by ethanol molecules both from surface and inside. And the backbones of the nanoribbons are destroyed more than those in water since a lot of holes are observed (Figure 4a,b) in the intermediate sample obtained after aging for 35 days. The (100) and (110) planes are perpendicular to the (001) plane, while the (101) plane is not, the fact that the more frequently observed the lattice fringes of (101) by the HRTEM images in Figure 5c,d are well consistent with the presence of intensified (101) peak appeared in the XRD patterns (Figure 7b,c). The results suggested that the ethanol molecules attacked the (001) and the

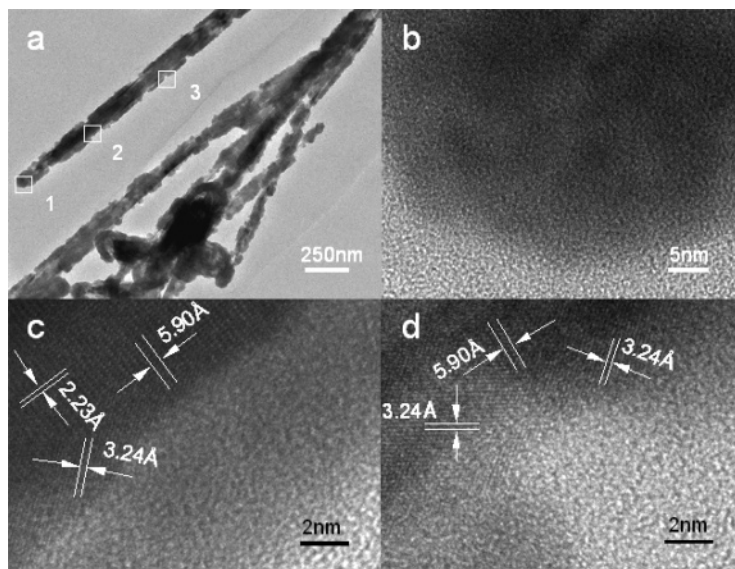


Figure 5. HRTEM images of the samples after erosion for 15 days in absolute ethanol: (a) typical morphologies of rotting nanoribbons; (b–d) HRTEM images taken in three areas along the backbone of the nanoribbon marked in part a, corresponding to the areas 1, 2, and 3, respectively.

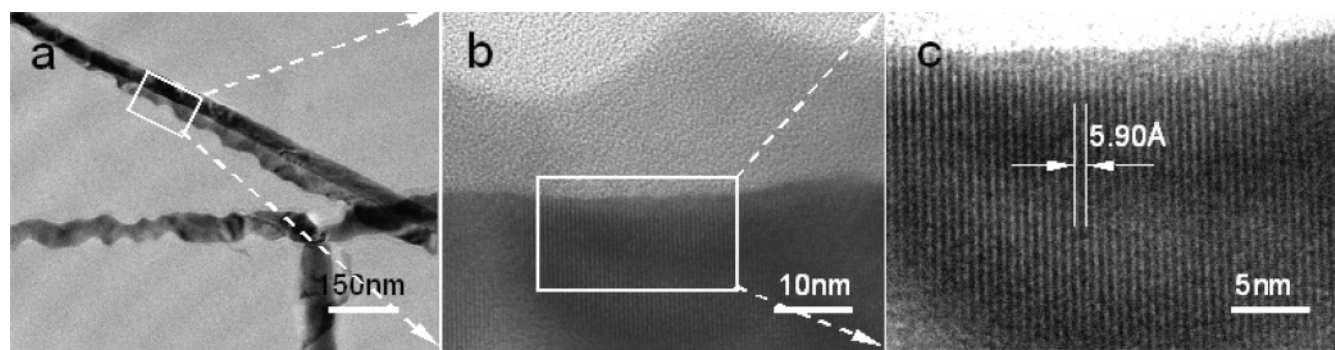


Figure 6. TEM and HRTEM images of the sample obtained after erosion for 15 days in deionized water, respectively: (a) typical morphology of rotten structures in water; (b) HRTEM image taken in the area marked in white rectangle in part a; (c) a magnified one selected in the area marked in part b.

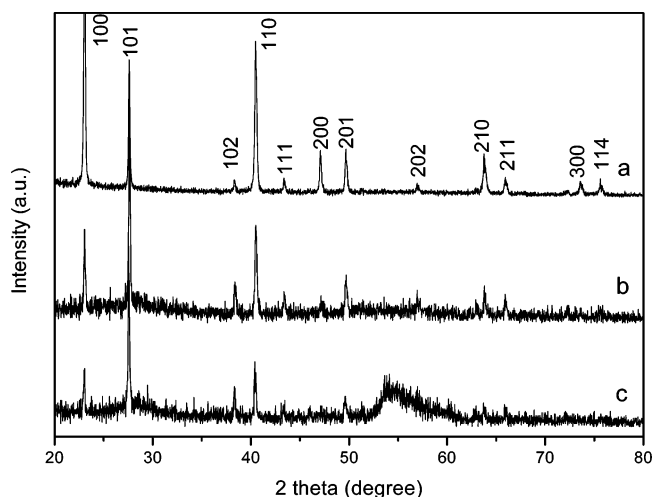


Figure 7. XRD patterns of time dependent samples during erosion of the intact nanoribbons in pure ethanol: (a) as-prepared tellurium nanoribbons; (b) nanoribbons after storing for 15 days; (c) nanoribbons after storing for 30 days.

planes which are perpendicular to it more severely than those planes which are not perpendicular to the (001), resulting in the much enhanced (101) peak appeared in the XRD pattern shown in Figure 7b,c. Second, with storing time prolonged, the crystallinity of the products becomes poor, implying the formation of an amorphous phase. The obvious poor crystallinity

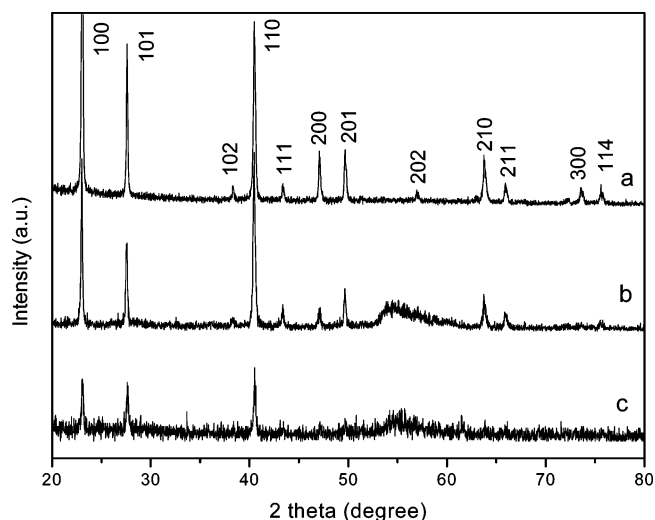


Figure 8. XRD patterns of time dependent samples during erosion of the intact nanoribbons in deionized water: (a) as-prepared tellurium nanoribbons; (b) nanoribbons after storing for 15 days; (c) nanoribbons after storing for 30 days.

of the samples after storing for a period demonstrated that the initial single crystalline nanobelts tend to be destroyed and to dissolve gradually in the solvent. In the mean time, the supersaturation of the solvable Te species in the solution will result in the formation of amorphous Te. The 2θ value around

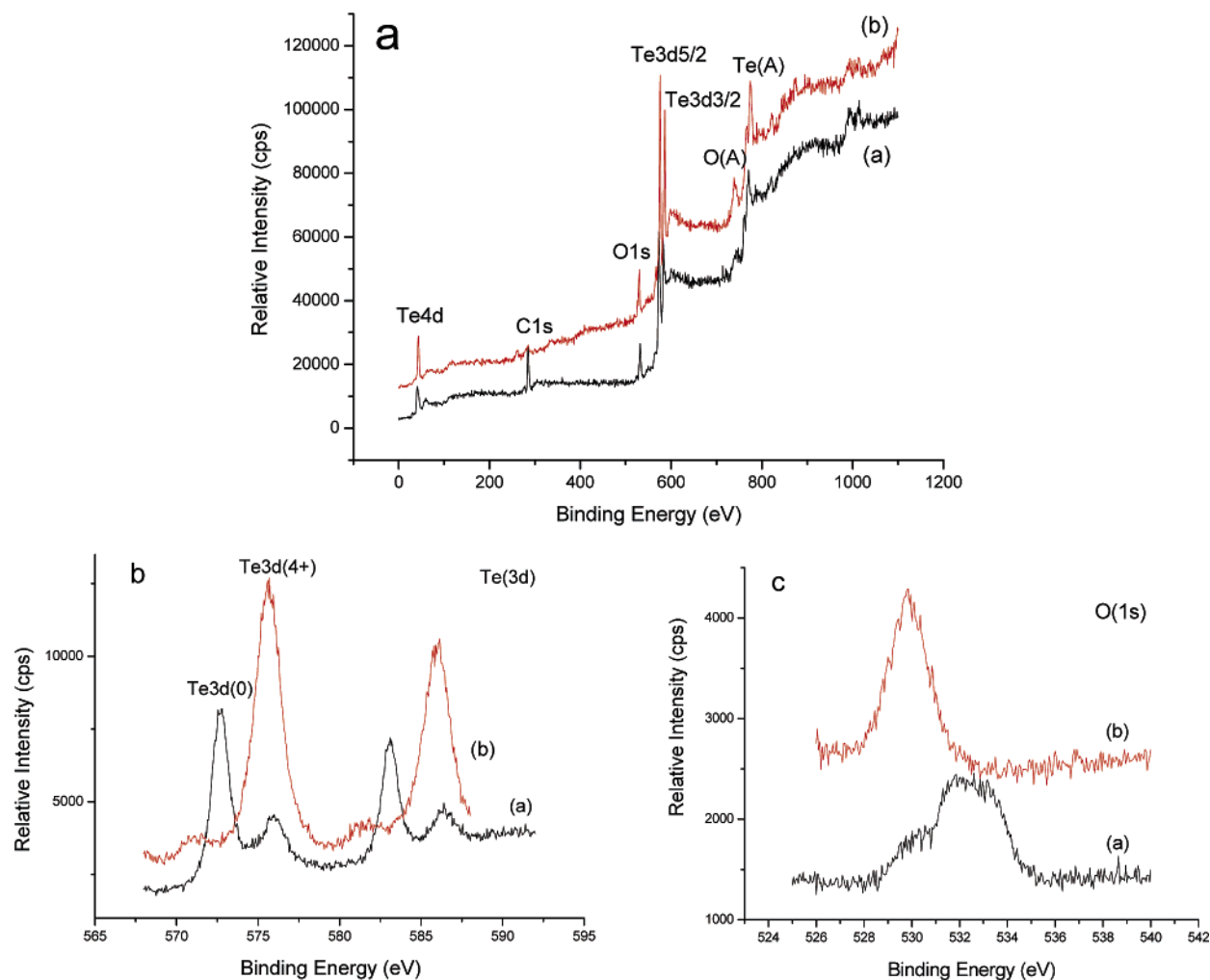


Figure 9. XPS spectra for the fresh sample (a, black) and the sample (b, red) after eroding for 4 months in ethanol: (a) surveys of the two samples; (b) survey of the Te 3d region in the two samples; (c) survey of the oxygen O 1s region in the two samples.

55° corresponds to the initial amorphous Te phase (Figure 7c), like that we observed in the intermediate product using amino acid controlled synthesis of highly crystallized Te nanostructures.¹⁴

In contrast, the intensity of each peak declined for the eroded nanoribbons in water, showing the same trend as that for the product obtained in ethanol. However, the relative intensities of three main peaks (100), (101), (110) (Figure 8b,c) for the eroded intermediates obtained in water remained the same as those for the initial intact nanoribbons (Figure 8a). The highly resolved lattice (intact (001) plane) image in Figure 6c clearly showed the continuous lattice fringes with a spacing of 5.90 Å. Even though the backbone of the nanoribbon was destroyed, however, the core part is still continuous single crystalline, resulting in that the XRD pattern is still kept as the same feature as that of initial nanoribbons (Figure 6a,b). An amorphous layer on the nanoribbon core was observed also (Figure 6b).

The XPS data measured on as prepared sample and the sample after eroding 4 months in ethanol is shown in Figure 9. The XPS quantitative analysis for the sample after eroding for 4 months indicated that the molar percentages of tellurium and oxygen are 27.5 at. % and 43.9 at. %, respectively. The obvious Te 3d peak shift shown in Figure 9b indicated that the different valence state of Te in the freshly prepared Te nanostructures and the eroded nanostructures. The spectrum (line a, black) in Figure 9b demonstrates the presence of both elemental tellurium 3d5/2 peak (572.70 eV)¹⁵ and a small amount of oxidized

tellurium (575.95 eV), accompanying the presence of O 1s peak (529.85 eV) in both spectra (Figure 9c), are consistent with that for TeO₂ reported by Garbassi et al.¹⁶ In addition, other two stripped peaks of the spectrum (curve a, black) in Figure 9c located at 531.85 and 533.35 eV, which denote -OH groups contained in metal hydroxides¹⁷ and H₂O,¹⁸ respectively. These results confirmed that the freshly prepared Te nanostructures tend to be oxidized in air to some extent, however, the Te nanostructures were seriously eroded and oxidized after long time storing in ethanol and amorphous TeO₂ will form.

In conclusion, we have demonstrated a facile route to prepare ultralong single crystal nanoribbons of tellurium in aqueous tetraethylene pentamine at low temperature. Tetraethylene pentamine acts not only as solvents and reducing reactants, but also as a soft template to shape one-dimensional structure. The shape evolution process of single crystalline nanoribbons has been investigated, in which the nanoribbons evolved from amorphous nanoparticles and nanowires finally to nanoribbons. On the basis of the detailed corrosion experiments, it has been confirmed that the as prepared Te nanoribbons are not stable if stored in solvents such as ethanol and water. The structure erosion in solvents is undertaking gradually attacked by solvent molecules with storing time prolonging. The poor crystallinity of the samples with prolonged storing time demonstrated that the initial single crystalline nanobelts tend to be destroyed and to dissolve in the solvent. In the mean time, the supersaturation of the solvable Te species in the solution will result in the

formation of amorphous Te in the solvents. In addition, the oxidization of the Te nanostructures and the newly formed amorphous tellurium will result in the formation of amorphous TeO₂ as a possible byproduct. The results demonstrated that the tellurium nanostructures synthesized by other methods could be also not stable in solution system and their storage after laboratory synthesis needs special attention. The stability of tellurium nanostructures synthesized by other routes in other solvents is being further examined and will be reported in due course.

Acknowledgment. S.-H.Y. expresses thanks for the funding support from the Centurial Program of the Chinese Academy of Sciences, the National Science Foundation of China (Nos. 20325104, 20321101, and 50372065), and the Scientific Research Foundation for the Returned Overseas Chinese Scholars, State Education Ministry.

References and Notes

- (1) (a) Kudryavstev, A. A. *The Chemistry and Technology of Selenium and Tellurium*; Collet's Ltd.: London, 1974. (b) Tangney, P.; Fahy, S. *Phys. Rev. B* **2002**, *14*, 279.
- (2) Zhao, A. W.; Ye, C. H.; Meng, G. W.; Zhang, L. D.; Ajayan, P. M. *J. Mater. Res.* **2003**, *18*, 2318.
- (3) Li, X. L.; Cao, G. H.; Feng, C. M.; Li, Y. D. *J. Mater. Chem.* **2004**, *14*, 244.
- (4) (a) Mayers, B.; Xia, Y. *Adv. Mater.* **2002**, *14*, 279. (b) Mayers, B.; Xia, Y. *J. Mater. Chem.* **2002**, *12*, 1875.
- (5) Mo, M. S.; Zeng, J.; Liu, X. M.; Yu, W.; Zhang, S. Y.; Qian, Y. T. *Adv. Mater.* **2002**, *14*, 1658.
- (6) (a) Liu, Z. P.; Hu, Z. K.; Xie, Q.; Yang, B. J.; Wu, J.; Qian, Y. T. *J. Mater. Chem.* **2003**, *13*, 159. (b) Liu, Z. P.; Li, S.; Yang, Y.; Hu, Z. K.; Peng, S.; Liang, J. B.; Qian, Y. T. *New J. Chem.* **2003**, *27*, 1748. (c) Liu, Z. P.; Hu, Z. K.; Liang, J. B.; Li, S.; Yang, Y.; Peng, S.; Qian, Y. T. *Langmuir* **2004**, *20*, 214.
- (7) Liu, Z. P.; Li, S.; Yang, Y.; Hu, Z. K.; Peng, S.; Liang, J. B.; Qian, Y. T. *New J. Chem.* **2003**, *27*, 1748.
- (8) Gautam, U. K.; Rao, C. N. R. *J. Mater. Chem.* **2004**, *14*, 2530.
- (9) Yu, H.; Gibbons, P. C.; Buhro, W. E. *J. Mater. Chem.* **2004**, *14*, 595.
- (10) Zhu, Y. J.; Hu, X. L. *Chem. Lett.* **2003**, *32*, 732.
- (11) Zhu, Y. J.; Wang, W. W.; Qi, R. J.; Hu, X. L. *Angew. Chem., Int. Ed.* **2004**, *43*, 1410.
- (12) Tang, Z. Y.; Wang, Y.; Sun, K.; Kotov, N. A. *Adv. Mater.* **2005**, *17*, 358.
- (13) Lu, Q. Y.; Gao, F.; Komarneni, S. *Adv. Mater.* **2005**, *16*, 1629.
- (14) He, Z. B.; Yu, S. H.; Zhu, J. P. *Chem. Mater.* **2005**, *17*, 2785.
- (15) Mandale, A. B.; Badrinarayanan, S. *J. Electron Spectrosc. Relat. Phenom.* **1990**, *53*, 87.
- (16) Garbassi, F.; Bart, J. C. J.; Petrini, G. *J. Electron Spectrosc. Relat. Phenom.* **1981**, *22*, 95.
- (17) Kishi, K.; Ikeda, S. *Bull. Chem. Soc. Jpn.* **1973**, *46*, 341.
- (18) Nefedov, V. I.; Gati, D.; Dzhurinskii, B. F.; Sergushin, N. P.; Salyn, Y. V. *Zh. Neorg. Khim.* **1975**, *20*, 2307.